Environmental Science & Technology

Article

pubs.acs.org/est

Characterization of the Mechanisms Controlling the Permeability Changes of Fractured Cements Flowed Through by CO_2-Rich Brine

H. Abdoulghafour,[†,*] L. Luquot,[†,‡] and P. Gouze[†]

[†]Géosciences, Université Montpellier, CNRS, UMR 5243, 34095 Montpellier cx 5, France

Supporting Information

ABSTRACT: Experiments were conducted to assess the potential impact of fractured well-cement degradation on leakage rate. Permeability was monitored while CO_2-enriched reservoir-equilibrated brine was flowed at constant rate through a single fracture in a class G cement core under conditions mimicking geologic sequestration environments (temperature 60 °C, pressure 10 MPa). The results demonstrate that, at least for the conditions used in the experiment, an initial leakage in a 42 μm aperture fracture (permeability = 1.5×10^{-10} m^2) can be self-mitigated due to the decrease of the fracture hydraulic aperture after about 15 h. This decrease results from the development of continuous highly hydrated amorphous Si-rich alteration products at the edge of the fracture and the dense carbonation of the bulk cement that mitigate the penetration of the alteration front.

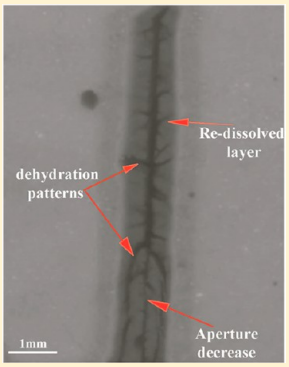

1. INTRODUCTION

Underground CO_2 sequestration often meets with public opposition mainly due to a negative perception of the controllability of the storage process. Critical questions concern the risk of CO_2 leakage and its negative impact on human health, valuable resources and environment.[1] Abandoned wells or wells used for the CO_2 injection and the reservoir monitoring are potential hydraulic and mechanical discontinuities linking the reservoir to the surface. Usually, sulfate-resistant, low viscosity Portland cements known as class G cements are used.[2,3] The well-completion cementation techniques benefit from tens of years of experience in the oil industry and have proven to be reliable for both oil and gas applications. However, for the application to CO_2 storage for which both highly acidic fluids are involved and long-term (hundreds of years) confinement is expected, the alteration of the sealing capacity of well cement annulus has been clearly identified as an important risk of CO_2 leakage from the reservoir to others permeable layers, including aquifers, and eventually to the surface.[4,5] Leakage pathways can occur along the casing-cement or the cement-caprock interfaces as well as through mechanically induced fractures within the bulk cement.

Portland cement mixed with water provides cement slurry composed mainly by amorphous hydrates and portlandite ($Ca(OH)_2$) which is the most crystallized phase. Calcium silicates hydrates (C−S−H) of general formulation $(CaO)_x(SiO_2)_y(H_2O)_z$, where $0.6 < x/y < 2$ and $1 < z < 4$, has crystallographic properties similar to tobermorite and jennite. The average composition in a fully hydrated cements is $x \cong 1.7$, $y \cong 1$ and $z \cong 4$. C−S−H phase is layered structures formed by imperfect nanocrystals (≤1.7 nm) with complex Si−OH and Ca−OH bonds. The Ca/Si ratio ranges from 0.7 to 2.3. They form the most important amorphous hydration products of cement based materials (60−70% of the fully hydrated cement paste) and control most of the properties of cement-based materials.[6,7]

Thermodynamic models (e.g., Beagi and Gherardi[8]) show that carbonic acid-rich water (eq 1) can dissolves most of the cement forming phases, and releases calcium that may combine with bicarbonates if present to precipitate calcium carbonates. Previous works using reactor or batch experiments, consisting of immersing samples of cement in water having compositions expected in the course of CO_2 storage and representative pressure and temperature conditions, confirmed the progressive carbonation of the samples.[9,10] All the previous studies converged toward the following cement alteration model: CO_2−rich water or brine diffuses into the cement and dissolves the cement bearing phases, especially portlandite (eq 2) and C−S−H (eq 3). The dissolution of portlandite and C−S−H consumes H^+ (pH raises) and produces free Ca^{2+} cations, which in turn will combine with CO_3^{2-} to form calcium carbonate (eq 4). The mass transfers can be modeled by the following set of reactions:

$$CO_2 + H_2O \leftrightarrow H_2CO_3 \leftrightarrow 2H^+ + CO_3^{2-} \quad (1)$$

$$Ca(OH)_2 + H^+ \leftrightarrow Ca^{2+} + OH^- + H_20 \quad (2)$$

$$(CaO)_x(SiO_2)_y(H_2O)_z + (x + 2y)H^+ \leftrightarrow xCa^{2+} + (SiO_2)_y + (OH^-)_{x+2y} \quad (3)$$

Received: March 26, 2013
Revised: August 12, 2013
Accepted: August 12, 2013
Published: August 12, 2013

$$Ca^{2+} + CO_3^{2-} \leftrightarrow CaCO_3 \quad (4)$$

$$CaCO_3 + H^+ \leftrightarrow Ca^{2+} + HCO_3^- \quad (5)$$

$$(SiO_2)_k + 2H_20 \leftrightarrow (SiO_2)_{k-1} + Si(OH)_4 \quad (6)$$

When the water-cement ratio is low, like in dead ends or diffusion dominated systems, carbonation reaction (eq 4) dominates.[11,12] However, for advection dominated mass transfers, the neo-formed calcite can be redissolved (eq 5). In addition, the polymerization of (ortho)silicic acids ($Si(OH)_4$) can take place (eq 6) at moderate pH and low Ca/Si ratio. For instance, Kutchko et al.[9] described such formation of silica-rich amorphous material at the surface of the sample immersed in a large volume of water (large water/fluid ratio). Accordingly, it has been often conjectured that the cement carbonation may decrease the cement permeability and favor the healing of microcracks.[11−13] Certainly, the settings studied in static or dynamic batch experiments mentioned above are far from the reality of a cement bulk in which fractures are flowed by CO_2-rich brine coming from the reservoir. Specifically it is important to study both the control of the calcite precipitation and subsequent redissolution on the alteration front pervasion and the extension of the development of silica-rich amorphous material. Recently, Walsh et al.[14] studied experimentally the coupled chemical and mechanical mechanisms controlling the permeability of an unconsolidated rough fracture. They linked the permeability decrease to the combined effect of the alteration of the fracture walls mechanical properties that triggered the collapsing of the two halves of the core and to the swelling of neoformed amorphous silicate layers. Fracture healing due to an increase of confining pressure was also discussed by Huerta et al.,[15] but these authors did not discussed the formation of silica-rich amorphous layer. Yet, the silica-rich amorphous material sustainability (or silica-gel) is low density, poorly cohesive materials with possible swelling properties depending on the composition of the fluid in which the polymerization occurs.

In the following, we report and discuss the results of a reactive flow through experiment in a sample of well-cement (class G Portland cement) during which both permeability and chemical effluent composition were monitored. In contrast to the experiments of Walsh et al.[14] works, the two halves of the fractures were tied together by their edges with fiberglass-loaded epoxy resin in order to avoid any mechanical effects. The experiments were performed under conditions mimicking geologic sequestration environments with a temperature of 60 °C and a pressure of 10 MPa, with the objective of determining the control of the carbonation and the silica-rich amorphous material growing on permeability.

2. MATERIALS AND METHODS

Preparation of the Fractured Cement Samples. A cement cylinder of size 40 mm diameter and 60 mm length was prepared using a class G Portland cement (Lafarge, Le Havre production unit, France) with a water-to-cement ratio of 0.40 following the provider recommendation. The composition of cement before hydration is 64.77 wt.% CaO, 21.36 wt.% SiO_2, 4.57 wt.% FeO, 3.56 wt.% Al_2O_3, 2.45 wt.% SO_3, 0.84 wt.% MgO, 0.59 wt.% P_2O_5, more low concentration (<0.2 wt.%) of TiO_2, Mn_2O_3, SrO and H_2O. The slurry was poured into a plastic, large aperture bottle and cured for a period of four months. Hydrated minerals formed during the curing were 50 wt.% CSH (Ca/Si = 1.65), 26 wt.% Portlandite ($Ca(OH)_2$), 10 wt.% Monosulfate ($Ca_4Al_2O_6(SO_4).14H_2O$,), 6.9 wt.% Ettringite ($Ca_6Al_2(SO_4)_3(OH)_{12}.26H_2O$), 3.8 wt.% Goethite (FeO(OH) with trace of Mn), 1.77 wt.% Hydrotalcite ($Mg_4Al_2(OH)_2CO$), 0.92 wt.% Brucite ($Mg(OH)_2$) and 0.19 wt.% undifferentiated Hémicarbonate. This composition was calculated using GEMS-PSI,[16] and was similar to that determined using thermogravimetric analysis (TGA) for portlandite and CSH. Subsequently, two cylinders of 9 mm diameter and 18 mm length were cored in the middle of the large size sample in order to avoid any boundary effects. Then, each core was sawn into two identical halves using a slow speed diamond blade. For each of the cylinders, noted hereafter G1 and G2, the two halves were assembled using a millimeter width stripe of Duralco 4525 epoxy resin (a high grade resin that ensures stable mechanical properties up to 260 °C and high resistance to aggressive inorganic chemicals) along the edges and calibrated wedges to control the gap between the two halves. Accordingly, the fracture aperture was maintained constant at the longitudinal edges of the sample independently of any confining pressure increase. This configuration mimics a smooth fracture of about 7 mm width and a quasi-homogeneous aperture.

Flow-Through Experiment. The experiment consisted in injecting CO_2-enriched brine throughout the fracture at constant flow rate. The experiments were performed using the ICARE-1 apparatus that was described in detail in Luquot and Gouze.[17] As a brief description, the experimental device consists of (1) the motorized dual-piston pump system that produces the flow of brine, (2) the motorized piston pump containing liquid-phase CO_2 cooled at 5 °C that deliver the amount of CO_2 required to reach the targeted CO_2 partial pressure, (3) the thermalized CO_2-brine mixing system that delivers a fully homogenized CO_2-enriched brine at the targeted temperature, (4) the temperature and pressure controlled confinement cell holding the sample into silicone jacket, and (5) the system composed of servo-controlled valves and hydro-pneumatic tanks that allows a continuous control of the outlet pressure while allowing recurrent fluid sampling. In the experiments, axial and radial pressures were both maintained at 112% of the inlet pressure using a mechanical pressure multiplier. Experiments were conducted at 60 ± 1 °C with pore pressure (back pressure) of 10 ± 0.2 MPa and flow rate Q = 2 ± 0.04 mL·min^{-1} (3.33 × 10^{-8} m^3·s^{-1}). These conditions were considered as realistic to reproduce average conditions of fractured well cement casing at the reservoir depth for CO_2 storage operations.

Initially the samples were saturated during 18 h (P = 10 ± 1 MPa and T = 20 °C), with cement equilibrated water at alkaline pH (pH = 12.6 ± 0.1). The cement equilibrated water was injected through the fractured samples at a constant flow rate of Q = 0.2 ± 0.004 mL·min^{-1} (3.33 × 10^{-9} m^3·s^{-1}). This cement-equilibrated water was prepared by mixing deionized water with 0.5 mols of NaCl and an excess of crushed cement for 5 weeks and filtered before use. Cement equilibrated brine was used to reproduce in situ reservoir fluid conditions surrounding the well cement before CO_2 rich fluid arrival due to leakage process. Then the system was heated up to 60 °C and flowed with the CO_2-enriched brine. This brine is a pH = 7.5 ± 0.1, Mg-calcite-equilibrated reservoir brine of composition C_{Ca} = 47.01 ± 1.41 mg·L^{-1}, C_{Mg} = 2.57 ± 0.12 mg·L^{-1}, C_{Na} = 12130 ± 14 mg·L^{-1}, C_{Cl} = 16 940.mg·L^{-1} ± 21 mg·L^{-1}, assumed representative of the reservoir prior to CO_2 injection. Note that the brine does

not contain any measurable silicon and is under-saturated with respect to calcite (saturation index, SI ≈ −5.2) and halite (SI ≈ −1.0) at 60 °C. Then, 0.43 ± 0.01 mol·L^{-1} (18.92 g·L^{-1}) of CO_2 was added, in order to obtain a CO_2 partial pressure (P_{CO2}) of 4. Three ±0.1 MPa. The resulting calculated pH (using Duan and Sun model)[18] was 3.12. The mixing of the liquid CO_2 and the brine is obtained by Taylor's dispersion effect in a 10 m-long, 0.5 mm diameter coiled tube maintained at 5 °C. This single phase fluid ($P_{CO2} < P$) is subsequently heated in a second 10m-long coiled tube to obtain the desired temperature (60 °C). Degassing occurs during effluent sampling, which makes the measurements of pH (Figure 2b) not very accurate and the measurement of $P_{CO2}$and therefore the calculation of outlet fluid SI's impractical.

Permeability Measurements. The pressure drop ΔP (Pa) between the inlet and the outlet of the fractured sample was continuously recorded using a high resolution differential pressure sensor (Rosemount 3051) in order to monitor the sample permeability k (m^2) during the experiment. For a planar fracture, the Hagen−Poiseuille cubic law (e.g., Zimmerman and Yeo),[19] relates the hydraulic aperture a_h to the pressure drop ΔP by

$$a_h = \sqrt[3]{\frac{12 \times \mu \times L \times Q}{w \times \Delta P}} \quad (7)$$

where μ is the fluid dynamic viscosity (Pa·s), L the fracture length (m), Q the volumetric flow rate (m^3·s^{-1}) and w the fracture width (m). Using eq 7, we calculated the initial effective hydraulic aperture a_h for G1 and G2, equal to 42 and 34 μm respectively.

The average velocity in the fracture is $U=Q/wa_h$ (i.e., 0.11 and 0.14 m·s^{-1} for G1 and G2, respectively) and the sample permeability (m^2) is given by $k = a_h^2/12$. Accordingly, the average time of the fluid in the fracture is in the order of 0.14 s. At the beginning of the experiment the permeability was 1.50 × 10^{-10} m^2 and 1.0 × 10^{-10} m^2 for G1 and G2 respectively. The mean Peclet number ($Pe = U \times a_h/2 \times d_0$) for both the experiments is 2950 ± 50, with d_0 the molecular diffusion equal to 8 × 10^{-10} m^2·s^{-1}.[20]

Fluid Chemical Analysis. Effluent was regularly sampled for chemical analysis of major ions (Ca, Si, Mg, Fe, Al) using inductively coupled plasma spectroscopy (ICP/AES). This enabled us to build reaction product breakthrough curves as the function of the elapsed time during the experiment. Furthermore, the pH of the effluent was monitored immediately after sample recovering to minimize the effect of degassing (i.e., pH increase due to CO_2 release). This measurement gives a fair evaluation of the pH variation with time but cannot be considered as a quantitative measure of the pH.

Structural Analysis of the Cement. Structural and chemical changes were investigated using an environmental scanning electron microscope (ESEM) equipped with back-scattered electron (BSE) detector and an energy-dispersive spectrometer (EDS). Powder X-ray diffraction (XRD) was used to identify crystallized phases. In complement, we used high resolution X-ray computed microtomography (XRMT)[14,21,22] to investigate phase and porosity distribution into the sample after the experiment. XRMT is a three-dimensional (3D) noninvasive visualization technique mapping the variation of X-ray attenuation within the object. The attenuation coefficient of a material depends on the energy of the incident X-ray beam, the chemical composition of the material (which relates closely to the atomic number Z), and the density ρ (i.e., the porosity). The XRMT data were collected using the ID19 beamline of the European Synchrotron Radiation Facility (ESRF). The samples were scanned using the white beam methodology (multi-chromatic) that produce a very dense beam. The image obtained through the scintillator was converted to digital data using a 2048 × 2048 pixels CCD (charge coupled device) FReloN (Fast Readout Noise) camera. The pixel size was 5.06 μm.

Standard complementary analysis based on thermogravimetry techniques (TGA/TDA) and bulk chemical analyses were performed in order to improve or confirm our description of the reaction mechanisms.

3. RESULTS

Experiment using G1 sample of duration 26 h (1550 min) was setup to analyze the alteration processes in details, while experiment using G2 sample was run for 5.5 h (330 min) in order to study the reaction front when the value of ΔC_{Si} ($\Delta C_{Si}= C_{Si}^{(out)} - C_{Si}^{(in)}$) begin to stabilize. We recall that both the experiments display similar Pe number independently of the difference in aperture, so that we can assume that the geochemical forcing is identical for the two experiments.

Permeability and Fluid Chemistry Changes. Figure 1 displays permeability changes during experiment G1 and G2.

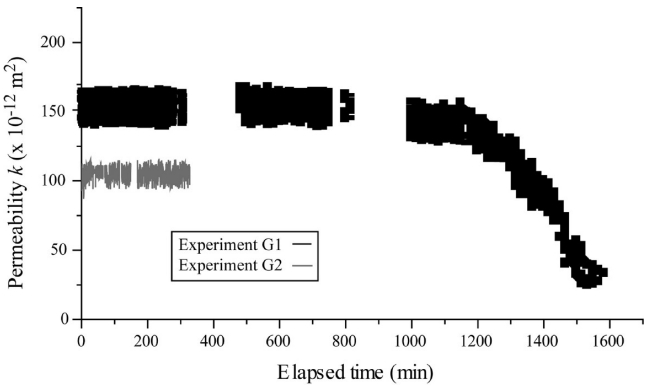

Figure 1. Permeability versus elapsed time for samples G1 (black) and G2 (gray).

Permeability remains constant all over the experiment G2 (i.e., from $0 \le t \le 330$ min). During experiment G1, the permeability also remains constant at the beginning of the experiment for the $0 \le t \le 900$ min. Then, for $t > 900$ min, permeability decreases from its initial value of ∼150 Darcy (1.49 × 10^{-10} m^2) to reach ∼24 Darcy (2.41 × 10^{-11} m^2) at the end of the experiment.

Figure 2.a displays the differential concentration value, for experiment G1, between the inlet and the outlet of the sample ΔC_i for i = Ca and Si, where $\Delta C_i = C_i^{(out)} - C_i^{(in)}$. We observed large positive values of ΔC_{Ca} and ΔC_{Si} during the first 100 min of the experiments, then the stabilization of ΔC_{Si} for the duration of the experiment at a value of 13.24 ± 0.3 mg·L^{-1}, while ΔC_{Ca}values continued to decrease strongly up to t = 330 min. For $330 \le t \le 1420$ min ΔC_{Ca}decrease rate ($-\partial C_{Ca}/\partial t$) was low and almost constant at a value of $-\partial C_{Ca}/\partial t$ = 11.2 × 10^{-3} mg·L^{-1}.min^{-1}. Then for $t > 1420$ min the decrease rate increased by more than 1 order of magnitude ($-\partial C_{Ca}/\partial t \cong 14 \times 10^{-2}$ mg·L^{-1}.min^{-1}). Note that Al and Fe concentration were

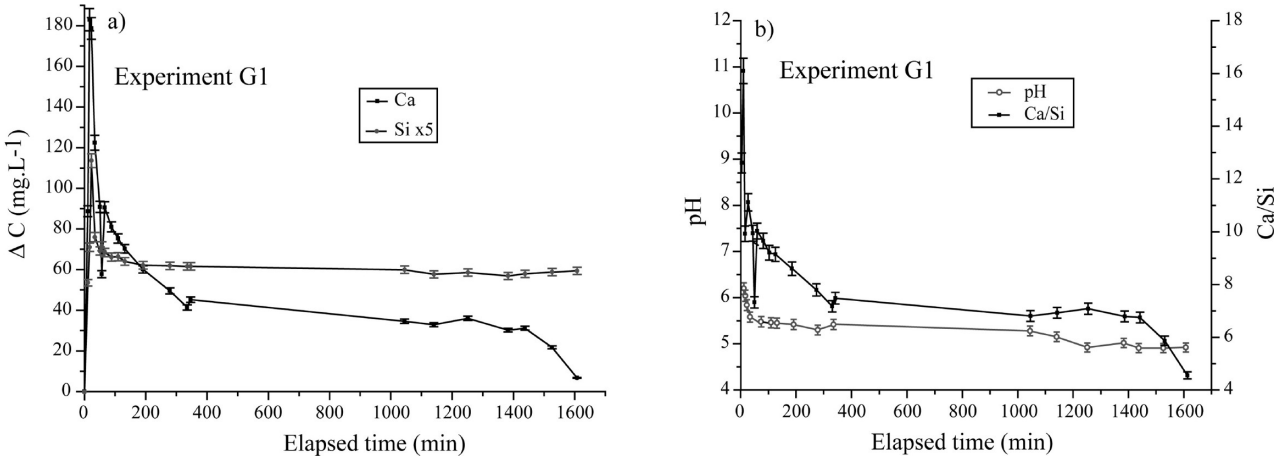

Figure 2. a: Differential $(\Delta C_i = C_i^{(out)} - C_i^{(in)})$ versus elapsed time for i = Ca and Si. Positive values of ΔC_i indicate the production of cation due to dissolution processes. b: outlet pH and Ca/Si ratio during experiment G1.

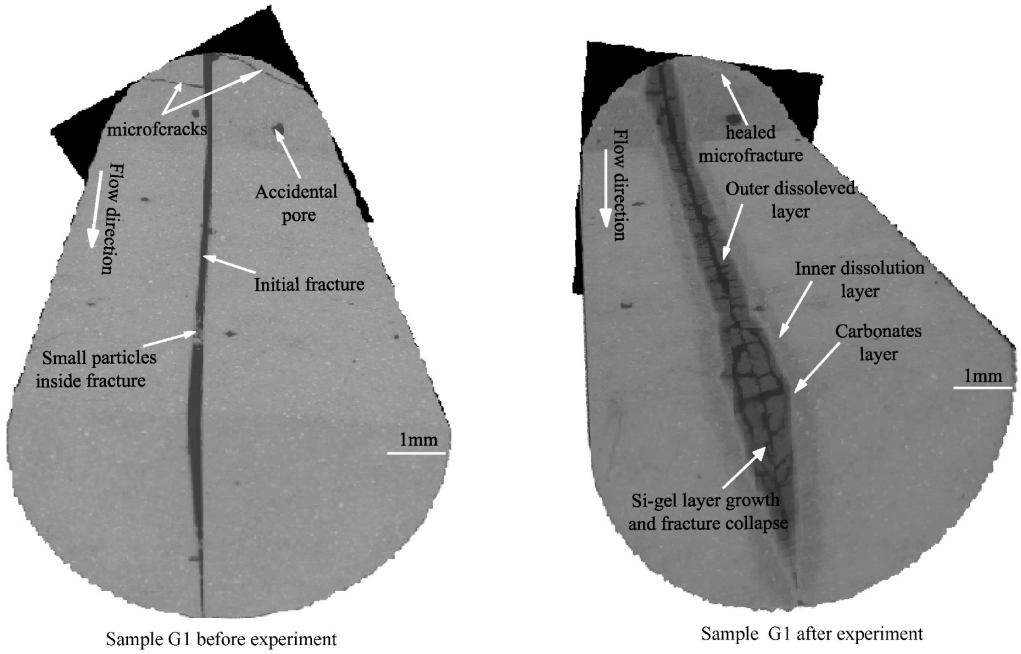

Figure 3. 3D XRMT images of sample G1 acquired before and after the experiment.

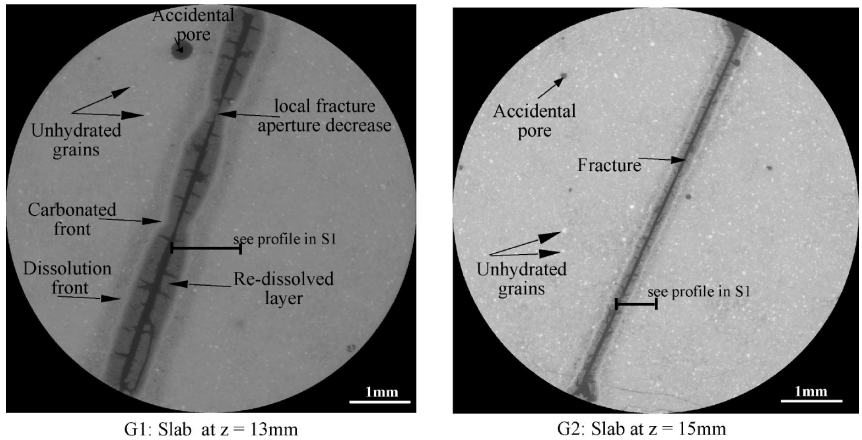

Figure 4. Numerical cross section in the XRMT image acquired after the experiment for G1 (t = 27.6 h) and G2 a (t = 5.4 h).

dx.doi.org/10.1021/es401317c | Environ. Sci. Technol. 2013, 47, 10332−10338

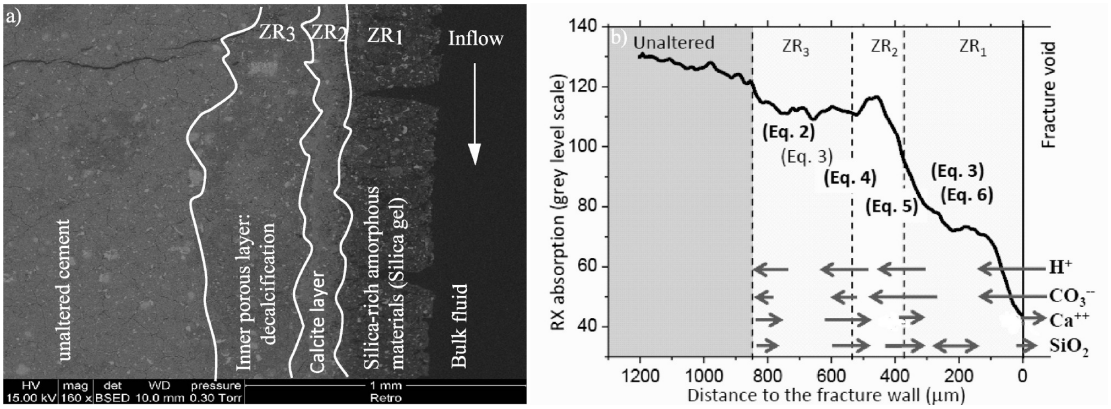

Figure 5. a: ESEM-BSE image of sample G1 after the experiment (t = 27.6 h) showing the different alteration layers controlled by the diffusion-reaction processes inside cement materials. b: schematic representation of the flux and reactions. Note that similar alteration patterns and involved reactions have been described previously.[9].

below the detection limit, that is, lower than 0.01 mg·L^{-1} and Mg concentration was quite constant along both experiments and equal to the inlet concentration.

The time-resolved pH and C_{Ca}/C_{Si} ratio are displayed in Figure 2b. We recall that the pH of the fluid entering the fracture was 3.45, whereas the equilibrium pH of the hydrated cement is around 12.6. The value of the outlet pH is higher than the calculated inlet pH and equal to 6.2 at the beginning of the CO_2-rich brine injection and decreases to values around 5.5 at t = 100 min. Then pH decreased almost linearly with time down to a value 4.8 at the end of the experiment. Comparing the pH curve with the ΔC_i curves (Figure 2a) shows an ubiquitous correlation between the pH and ΔC_{Si}. Conversely, the C_{Ca}/C_{Si} ratio curve shape was rapidly (i.e., t > 100 min) controlled by the value of Ca (or ΔC_{Ca}) curve because of the stationary value of Si (or ΔC_{Si}) for t > 100 min.

Characterization of the Alteration Patterns. The thickness of the three different alteration layers appears to be almost the same from the inlet to the outlet (Figure 3). This indicates that the CO_2-enriched brine concentration kept its reactivity capacity all along the sample length, or in other words that the flow was sufficiently rapid to promote fairly uniformly distributed reactions along the fracture. Accordingly, the reactions in the vicinity of the fracture walls occurred far from equilibrium. Figures 4 and Supporting Information S1 allows comparing the alteration layer thicknesses between the two experiments. As expected the thickness of the different layers are thinner in G2 than in G1 because of the experiment duration was almost 5 times shorter for G2 than for G1. The sum of the three alteration layers was 0.85 ± 0.18 mm and 0.28 ± 0.05 mm for G1 and G2 respectively.

The ESEM-BSE image presented in Figure 5 gives more details of the different alteration layers due to the CO_2-enriched brine flow for G1. The composition of the alteration layer deduced from ESEM-EDS analysis and expressed in terms Ca/Si and Ca/C ratios are given in SI Figure S2. Starting from the fracture side, the first alteration layer is a highly porous layer mainly constituted by hydrated silica gel with Fe-rich zones giving the typical orange color observed by optical microscopy and very low calcium content. The cracks almost perpendicular to the fracture plane and uncorrelated with any changes of the geometry of the other alteration layers are attributed to dehydration structures occurring after the sample is removed from the experimental setup. Accordingly, the porosity of this layer is probably even larger than that observed on the zone delimited by the cracks. The layer thickness is 0.38 ± 0.05 mm and is adjoined to a much denser, that is, lower porosity, layer of thickness of 0.15 ± 0.02 mm enriched in calcium carbonate (XRD and thermo-gravimetric data analysis indicate that the calcium carbonate is calcite). The next observed alteration layer embedded between the dense calcium rich layer and the unaltered cement is depleted in calcium and displays higher porosity than the unaltered cement. Its thickness is 0.35 ± 0.05 mm.

4. DISCUSSION

Cement Alteration and Permeability Changes. During experiment G1 (Figure 2), for the first 30 min or so, calcite precipitation was not efficient and the high concentration of Ca and Si denotes the calcium released from the C−S−H and portlandite dissolution and the silicon released by C−S−H dissolution. Then, for 30 ≤ t ≤ 300 min the C_{Ca}/C_{Si} ratio decreased rapidly toward a value of 7.1 while ΔC_{Si} stayed constant denoting a decrease of the calcite dissolution rate relative to the dissolution of both portlandite and CSH. For 300 < t < 1450 min the system appeared to be at steady state; C_{Ca}/C_{Si} is almost constant. For the last few hours C_{Ca}/C_{Si} decreased more noticeably as ΔC_{Ca} denoting an increase of the calcite precipitation or decrease of calcite redissolution. The steady-state of the outlet Si concentration ΔC_{Si} indicates that the precipitation of the Si-rich amorphous layer control the total Si mass balance.

A substantial result of these experiments is that permeability remained constant at the beginning of the experiment during the first sixteen hours for experiment G1 (~900 min) and all over the experiment G2 (330 min). This result matches those reported by Luquot et al.,[22] who performed CO_2-rich brine injection through fractured standard portland cement for comparable temperature, pressure and low rate conditions. These authors (op. cit.) measured similar constant permeability during all over the experiment (~300 min) and observed the formation of a Si-rich layer of similar thickness than the one measured here for G2.

For both G1 and G2 experiments, the constant permeability occurs while the effluent concentration changes noticeably. Moreover, no clear correlation is noted when the permeability started to decrease (from 1.49 × 10^{-10} m^2 to 2.41 × 10^{-11} m^2) for G1. Yet, we notice a delayed correlation (~2 h) between the

permeability drop and the strong depletion of the fluid in Ca. The decrease of permeability denotes a decrease of the effective hydraulic aperture and implies a volume expansion of solid phase.[14] However the net mass balance indicated matter removal during the entirety of the experiment. Clearly the outer alteration layer, that is. the growing layer of amorphous silica-rich material controls the effective hydraulic aperture and therefore the permeability of the sample. During the first 900 min of the experiment, this material maintained a constant hydraulic aperture independently of bulk alteration of the sample (the same is observed for experiment G2). We conjecture a progressive expansion of the layer during the experiment. According to eq 7 the fracture hydraulic aperture a_h would have changed from 42 μm for $0 \leq t \leq 900$ to about 20.1 μm at the end of the experiment, that is, a decrease of about 52.1.7% of the fracture volume. For comparison with the experiments of Walsh et al.[14] where the two halves of the core were free to move closer while the fracture walls were altered, the permeability decrease measured for G1 and G2 can be attributed to the fracture feeling material only. The effect of calcium carbonates precipitation on permeability decrease was neglected as acidified fluid redissolved partially the calcite layer. Thus the main cause of Ca drop on the effluent is the proximity of the diffusion front over the fluid renewal, which minimizes the Ca rich material dissolution. It could be assumed that minor calcium carbonates precipitate within silica gel pores.

The polymerization of silicic acid is pH dependent. In an alkaline solution (pH > 9), monosilicic acid does not polymerize and the polymerization is slower in acid solutions (pH < 5). Albeit being generally considered as an inconsequential process, amorphous silica growth on cement material exposed to acidic environments, for instance with HCl, was often observed.[15,23−25] According to Iler,[26] rapid silica gelling occurs for pH ranging from 5 to 6 which is the value measured for the outlet fluid (Figure 2b), while the average pH within he fracture should be comprised between this value and that of the inlet fluid (i.e., pH 3.12). Such pH values smaller than 5 do not correspond to the optimal conditions for rapid formation of silica amorphous layer, however, a strong pH gradient normal to the flow direction is expected due to the diffusion profile triggered by the reactions with the cement that is characterized by a pH of around 13. As a result, the occurrence of pH values ranging from 5 to 6 within the forming silica amorphous material is highly probable.[27]

This rationalizes the formation of the silica-gel, but does not explain the sudden drop of permeability starting at $t \cong 900$ min. Exploring the origin of this permeability decrease implies investigating the factors that could control the increase of the silica-gels production rate or the decrease of its density due to an increase of water retention. As mentioned above, we observed that the drop of permeability started shortly before the Ca concentration began to drop which is attributed to the progressive thickening of the silica amorphous layer that in turn increase the diffusion time the reactants and products (for instance Ca) involved in calcite alteration reactions. Eventually, both decrease with similar relative time-dependent rates emphasizing the close relation between the apparent rate of cement chemical alteration (for instance the calcite dissolution) and the thickness of the amorphous silica layer.

To the best of our knowledge, there is not any published data concerning the effect of the Ca concentration on the density (ranging from 0.6 to 0.7 $kg{\cdot}L^{-1}$) of silica-gels. However, Gaboriaud et al.[28] measured noticeable differences in both the size of the fractal aggregate forming sol−gels and the kinetics depending on the Ca content. Also not conclusive, these results emphasize the possible correlation between the permeability and the calcium content, which is in turn controlled by the calcite dissolution. Further experiments with different calcium content in the fluid would be necessary to explore this assumption.

Well Cement Integrity and Leakage Risk. Previous works (Kutchko et al.[29] and references herein) showed that significant mass transfers can alter cement integrity in CO_2 storage conditions. The dynamic of formation of the complex multilayered dissolution−precipitation fronts depends on the cement quality and curing and water/cement ratio.[5] Weak bond along cement/casing and cement/rock interfaces as well as fractures constitute the main identified pathways for CO_2 leakage. Whether the permeability of these hydraulic discontinuities will be enhanced or mitigated by the cement alteration products is a critical issue for assessing the risk of leakage. Very few published data concerning well cement having been in contact with CO_2 for several years in reservoir conditions are available. Yet, Carey et al,[30] described the alteration zones observed on samples recovered from a real wellbore cement (Portland cement) exposed to CO_2 during 30 years at 54 °C and 18 MPa at the SACROC unit in Texas. Observations indicated that well cement maintained its sealing properties characterized by a very low bulk permeability of few millidarcies. The studied samples were not fractured; however, the study of the interfaces between the caprock displayed alteration patterns including regions with high porosity formed by silicate deposits with few carbonates deposits.

Here we conducted experiments to assess the potential impact of fractured well-cement degradation on leakage rate that is controlled by the permeability of the fracture. The results discussed above emphasize the role of the amorphous silica-rich material that develops inside the fracture caused by C−S−H decalcification forming long silicates hydrates chains. Nasvi et al.[31] showed that the permeability of geopolymer (including silica gel) is noticeably smaller than unaltered Portland cement permeability. The efficiency of this material to seal the fracture by overgrowing or swelling in the fracture was demonstrated here for standard CO_2 storage conditions. This fast and apparently sustainable mechanism seems to be efficient to mitigate the rate of CO_2 leakage through fractures initially of few tens of μm. Nevertheless, this silica gel is a loose, low density material with Young's (tensile) modulus of about 0.85 ± 0.10 GPa, and a shear modulus of about 0.50 ± 0.05 GPa, that is, about 30 and 5 time less than the cement, respectively.[32,33] The question of the sustainability of the fracture sealing (i.e., its resistance to hydrodynamic erosion and or mechanical effect) in case of flow rate increase is open, and would require further experiments. The efficiency of the silica-gel in higher aperture fracture must be tested as well.

■ ASSOCIATED CONTENT

Supporting Information

Gray scale profile (XRMT attenuation), and Ca/Si−Ca/C ratios (in atom%) from BSE-EDS images and analysis. This material is available free of charge via the Internet at http://pubs.acs.org.

■ AUTHOR INFORMATION

Corresponding Author

*Corresponding author.

Present Address
‡IDAEA-CSIC/CIMNE Barcelona, C/Jordi Girona 18-26, 08034 Barcelona, Spain

Notes
The authors declare no competing financial interest.

■ ACKNOWLEDGMENTS

This work was supported by the PANACEA project (grant agreement n°282900) as part of the European Community FP7/ENERGY.2011.5.2-1 research program on long-term fate of geologically stored CO_2 and by the French Research National Agency (ANR) through the "Captage et stockage du CO_2" program (project CO-LINER n°ANR-08-PCO$_2$-004). The authors thank P. Tafforeau and E. Boller from ESRF−ID19 for their significant help in acquiring high quality X-ray microtomography images. H.A. thansk the Islamic development bank (ISDB) for the PhD grant allocation.

■ REFERENCES

(1) Oldenburg, C. M.; Bryant, S. L.; Nicot, J. P. Certification framework based on effective trapping for geologic carbon sequestration. *Int. J. Greenhouse Gas Control.* **2009**, *3*, 444−457.
(2) Robins, N. S. Borehole cements and the down hole environment − *a review*. *Q. J. Eng. Geol. Hydrogeol.* **1986**, *19*, 175−81.
(3) Barron, A. R.; http://creativecommons.org/licenses/by/2.0/ Connexions module:m16444 Version 1.10 (**26.06.09**) 7:42 pm GMT-5.
(4) Celia, M. A.; Nordbotten, J. M.; Court, B.; Dobossy, M.; Bachu, S. Field-scale application of a semi-analytical model for estimation of CO_2 and brine leakage along old wells. *Int. J. Greenhouse Gas Control.* **2011**, *5*, 257−269.
(5) Nordbotten, J. M.; Kavetski, D.; Celia, M. A.; Bachu, S. Model for CO_2 leakage including multiple geological layers and multiple leaky wells. *Environ. Sci. technol.* **2009**, *43* (3), 743−749.
(6) Powers T. C.; Brownyard, T. L. Studies of the physical properties of hardened Portland cement paste, 1948, PCA Bulletin 22.
(7) Diamond, S. The microstructure of cement paste and concrete - a visual primer. *Cem. Concr. Compos.* **2004**, *26*, 919−933.
(8) Biagi, S.; Gherardi, F. CO_2 storage in a depleted gas reservoir in Italy: modeling the diffusion of CO_2-rich fluids within the wellbore cement of abandoned well. In *Water-Rock Interaction*; Brinkie, P., Torres-Alvarado, I. S, Eds.; CRC Press, Taylor & Francis Group: London, 2010; pp 843−850, ISBN 978-0-415-60426-0.
(9) Kutchko, B. G.; Strazisar, B. R.; Dzombak, D. A.; Lowry, G. V.; Thaulow, N. Degradation of well cement by CO_2 under geologic sequestration conditions. *Environ. Sci. Technol.* **2007**, *41* (12), 4787−4792.
(10) Rimmelé, G.; Barlet-Gouédard, V.; Porcherie, O.; Goffe, B.; Brunet, F. Heterogeneous porosity distribution in Portland cement exposed to CO_2-rich fluids. *Cem. Concr. Res.* **2008**, *38*, 1038−1048.
(11) Liteanu, E.; Spiers, C. J. Fracture healing and transport properties of wellbore cement in the presence of supercritical CO_2. *Chem. Geol.* **2010**, *281*, 195−210.
(12) Wigand, M.; Kaszuba, J. P.; Carey, J. W.; Hollis, W. K. Geochemical effects of CO_2 sequestration on fractured wellbore cement at the cement/caprock interface. *Chem. Geol.* **2009**, *265*, 122−133.
(13) Bachu, S.; Bennion, D. B. Experimental assessment of brine and/or CO_2 leakage through well cement at reservoir conditions. *Int. J. Greenhouse Gas Control* **2009**, *3*, 494−501.
(14) Walsh, S. D.; Du Frane, W. L.; Mason, H. E.; Carrol, S. A. Permeability of wellbore fractures following degradation by carbonated brine. *Rock Mech. Eng. Geol.* **2013**, *46*, 455−464.
(15) Huerta, N. J.; Hesse, M. A.; Bryant, S. L.; Strazisar, B. R.; Lopano, C. L. Experimental evidence for self-limiting reactive flow through a fractured cement core: Implications for time dependent wellbore leakage. *Environ. Sci. Technol.* **2013**, *47*, 269−275.
(16) Kulik, D. A.; Wagner, T.; Dmytrieva, S. V.; Kosakowski, G.; Hingerl, F. F.; Chudnenko, K. V.; Berner, U. GEM-Selektor geochemical modeling package: revised algorithm and GEMS3K numerical kernel for coupled simulation codes. *Comput. Geosci.* **2003**, *17*, 1−24.
(17) Luquot, L.; Gouze, P. Experimental determination of porosity and permeability changes induced by massive injection of CO_2 into carbonates reservoirs. *Chem. Geol.* **2009**, *265*, 148−159.
(18) Duan, Z.; Sun, R. An improved model calculating CO_2 solubility in pure water and aqueous NaCl solutions from 273 to 533 K and from 0 to 2000 bar. *Chem. Geol.* **2003**, *193*, 257−271.
(19) Zimmerman, R. W.; Yeo, I. W. Fluid Flow in Rock Fractures: From the Navier-Stokes Equations to the Cubic Law. In: Faybishenko B., Witherspoon P. A., Benton S. M., eds. Dynamics of Fluids in Fractured Rock. *AGU Geophys Mono.* 2000, *122*, 213-24.
(20) Samson, E.; Marchand, J.; Snyder, K. A. Calculation of ionic diffusion coefficients on the basis of migration test results. *Mater. Struct.* **2003**, *36*, 156−165.
(21) Jung, H. B.; Jansik, D.; Um, U. Imaging wellbore cement degradation by carbon dioxide under geologic sequestration conditions using X-ray Computed Microtomography. *Environ. Sci. Technol.* **2013**, *47* (1), 283−289, DOI: 10.1021/es3012707.
(22) Luquot, L.; Abdoulghafour, H.; Gouze, P. Hydro-dynamically controlled alteration of fractured Portland cements flowed by CO_2-rich brine. *Int. J. Greenhouse Gas Control.* **2013**, *16*, 167−179.
(23) Taylor, H. F. W. *Cement Chemistry*; Academic Press: London, 1990.
(24) Dunster, A. M. An investigation of carbonation of cement paste using trimethylsililation. *Adv. Cem. Res* **1989**, *2* (7), 99−106.
(25) Duguid, A.; Scherer, G. W. Degradation of oil well cement due to exposure to carbonated brine. *Int. J. Greenhouse Gas Control.* **2010**, *4*, 546−560.
(26) Iler, R. K. *The Chemistry of Silica, Solubility, Polymerization Colloid and Surface Properties and Biochemistry*; Cornell University Press, 1955.
(27) Leemann, A.; Lothenbach, B.; Siegrist, H.; Hoffmann, C. Influence of water hardness on concrete surface deterioration caused by nitrifying biofilms in wastewater treatment plants. *Int. Biodeterior. Biodegrad.* **2010**, *64*, 489−498.
(28) Gaboriaud, F.; Nonat, A.; Chaumont, D.; Craievich, A. Aggregation processes and formation of silico-calco-alkaline gels under high ionic strength. *J. Colloid Interface Sci.* **2002**, *253*, 140−149.
(29) Kutchko, B. G.; Strazisar, B. R.; Lowry, G. V.; Dzombak, D. A.; Thaulow, N. Rate of CO_2 attack on hydrated Class H well cement under geologic sequestration conditions. *Environ. Sci. Technol.* **2008**, *42* (16), 6237−6242.
(30) Carey, J. W.; Wigand, M.; Chipera, S. J.; Wolde Gabriel, G.; Pawar, R.; Lichtner, P. C.; Wehner, S. C.; Raines, M. A.; Gurthrie, G., Jr. Analysis and performance of oil well cement with 30 years of CO_2 exposure from SACROC Unit, West Texas,USA. *Int. J. Greenhouse Gas Control.* **2007**, *1*, 75−88.
(31) Nasvi, M. C. M.; Ranjith, P. G.; Sanjayan, J. The permeability of geopolymer at down-hole stress conditions: Application for carbon dioxide sequestration well. *Applied Energy.* **2013**, *102*, 1391−1398.
(32) Spagnol, S. Transfert conductif dans des aérogels de silice du milieu nanoporeux autosimilaire aux empilements granulaires. PhD. Dissertation, Université de Toulouse, France, 2007.
(33) Adachi, T.; Sakka, S. Dependance of the elastic moduli of porous silica gel prepared by the sol gel method on heat treatment. *J. Mater. Sci.* **1990**, *25*, 4732−4737.